Published in final edited form as:
Glia. 2010 November 1; 58(14): 1669–1685. doi:10.1002/glia.21039.

Activation of PPAR-γ and PTEN Cascade Participates in Lovastatin-mediated Accelerated Differentiation of Oligodendrocyte Progenitor Cells

Ajaib S Paintlia[#],
Darby Children's Research Institute, Department of Pediatrics, Medical University of South Carolina

Manjeet K Paintlia[#],
Darby Children's Research Institute, Department of Pediatrics, Medical University of South Carolina

Avtar K Singh, and
Department of Pathology and Laboratory Medicine Ralph H. Johnson VA Medical Center, Charleston, South Carolina 29425

Inderjit Singh
Darby Children's Research Institute, Department of Pediatrics, Medical University of South Carolina

Abstract

Previously, we and others documented that statins including—lovastatin (LOV) promote the differentiation of oligodendrocyte progenitor cells (OPCs) and remyelination in experimental autoimmune encephalomyelitis (EAE), an multiple sclerosis (MS) model. Conversely, some recent studies demonstrated that statins negatively influence oligodendrocyte (OL) differentiation *in vitro* and remyelination in a cuprizone-CNS demyelinating model. Therefore, herein, we first investigated the cause of impaired differentiation of OLs by statins *in vitro* settings. Our observations indicated that the depletion of cholesterol was detrimental to LOV treated OPCs under cholesterol/serum-deprived culture conditions similar to that were used in conflicting studies. However, the depletion of geranylgeranyl-pp under normal cholesterol homeostasis conditions enhanced the phenotypic commitment and differentiation of LOV-treated OPCs ascribed to inhibition of RhoA-Rho kinase. Interestingly, this effect of LOV was associated with increased activation and expression of both PPAR-γ and PTEN in OPCs as confirmed by various pharmacological and molecular based approaches. Furthermore, PTEN was involved in an inhibition of OPCs proliferation via PI3K-Akt inhibition and induction of cell cycle arrest at G1 phase, but without affecting their cell survival. These effects of LOV on OPCs *in vitro* were absent in the CNS of normal rats chronically treated with LOV concentrations used in EAE indicating that PPAR-γ induction in normal brain may be tightly regulated — providing evidences that statins are therapeutically safe for humans. Collectively, these data provide initial evidence that statin-mediated activation of the PPAR-γ — PTEN cascade participates in OL differentiation, thus suggesting new therapeutic-interventions for MS or related CNS-demyelinating diseases.

Address for correspondence:Inderjit Singh, PhD, Medical University of South Carolina, Department of Pediatrics, 173 Ashley Avenue, Charleston, SC 29425 Tel # (843) 792-7542; Fax # (843) 792-7130 singhi@musc.edu.
[#]These authors contributed equally to this study.

Keywords

Lovastatin; EAE/MS; oligodendrocyte progenitors; PPAR-γ/PTEN; RhoA-ROCK; Differentiation; remyelination

INTRODUCTION

Demyelination of neuronal axons is responsible for neurological deficits in many central nervous system (CNS) demyelinating diseases including multiple sclerosis (MS) (Prineas et al. 1993). It is ascribed to the loss of oligodendrocytes (OLs) and their progenitor cells (OPCs) due to recurring inflammatory attacks in the brain. Neurological deficits usually disappear in MS patients by spontaneous remyelination of axons by myelinating OLs present in acute lesions, while they persist in some patients due to failed remyelination especially in chronic lesions (Jeffery and Blakemore 1997; Prineas et al. 1993). In chronic lesions, axons are non-responsive to OPCs (Chang et al. 2002; Dawson et al. 2000) due to the accumulation of inhibitory molecules or degraded myelin (Charles et al. 2002). These inhibitory molecules block the differentiation of OPCs into myelinating OLs (Back et al. 2005; Kotter et al. 2006) via increased activation of RhoA and protein kinase C (Baer et al. 2009). Therefore, we proposed that the understanding of mechanism by which an agent influences OPC differentiation and remyelination would hold promise for designing of new therapeutic interventions for CNS demyelinating diseases.

Presently, a therapy is needed that can alleviate MS pathogenesis by targeting both demyelination and remyelination mechanisms in the CNS. Previous studies by us and others established the anti-inflammatory (Pahan et al. 1997) and immunomodulatory (Nath et al. 2004; Paintlia et al. 2004; Stanislaus et al. 2001; Youssef et al. 2002) activities of statins participating in the attenuation of experimental autoimmune encephalomyelitis (EAE), an MS animal model. Subsequently, we reported that lovastatin (LOV) enhances the differentiation of OPCs into myelinating OLs in mixed glial cultures and remyelination in EAE model that could be attributed to direct/indirect consequence of immune-modulation (Paintlia et al. 2005). Later, Miron *et al*. (2007) documented that statin directly influences OPC differentiation via inactivation of RhoA. RhoA inactivation in LOV treated OPCs was ascribed to the lowering of cellular geranylgeranyl-pp (GGPP), but not farnesyl-pp (FPP) (Miron et al. 2007; Paintlia et al. 2008). Recently, the peroxisome proliferator-activated receptor (PPAR)-γ has also been implicated in statin-mediated differentiation of OPCs (Sim et al. 2008); however, the mechanism responsible for its activation is not clear. Moreover, these studies provide evidence of an inverse relationship between RhoA and PPAR-γ activities in statin-treated OPCs.

Since cholesterol as the main constituent of myelin lipids produced by OLs, is required for myelin formation in the CNS (Saher et al. 2005), considering statins as MS therapeutics raise legitimate concerns. In addition, few recent studies documented that statins impede the differentiation of OLs *in vitro* and block remyelination in a cuprizone-CNS demyelinating model (Klopfleisch et al. 2008; Maier et al. 2008; Miron et al. 2009). These studies are in contrast to previous reports that document statin-mediated enhanced differentiation of OPCs *in vitro* (Miron et al. 2007; Paintlia et al. 2005; Paintlia et al. 2008; Sim et al. 2008) and induction of CNS remyelination in an EAE paradigm (Paintlia et al. 2005; Paintlia et al. 2008). Therefore, in this study, we sought to address the mechanism behind such observed negative effects of statins on OPCs *in vitro* settings. Our findings clearly document that statin treatment enhances the differentiation of OPCs in the presence of FBS, but not under cholesterol/FBS deprived culture conditions similar to that were used in conflicting studies. Next, we documented that GGPP depletion mediated inhibition of RhoA-Rho kinase

(ROCK) — activates PPAR-γ and the tumor suppressor phosphatase and tensin homolog (PTEN) signaling cascade in LOV treated OPCs which participate in their differentiation into OLs (Fig. 1). Finally, we demonstrated that statins are safe to treat CNS demyelinating diseases.

MATERIALS AND METHODS

Chemicals and Reagents

Unless otherwise stated, all chemicals were purchased from Sigma (St. Louis, MO). LOV, GGTI-298, FTI-277, Y27632, ciglitazone (CGN), 15-deoxy-prostaglandin J2 (15d-PGJ2), GW9662, Akt inhibitor, wortmannin and cholesterol were purchased from Calbiochem (La Jolla, CA). Membrane-permeable C3 exoenzyme (C3-EXZ) was purchased from Cytoskeleton, Inc (Denver, CO). DMEM (4.5 g/L glucose), fetus bovine serum (FBS), and laminin-2 were obtained from Invitrogen (Carlsbad, CA). Anti-PPAR-γ, -PTEN, -phosphorylated PTEN, -Akt, -phosphorylated Akt (ser), -cyclooxygenase-2 (COX-2), -phosphorylated extracellular signal regulated-kinase (ERK) 44/42, -phosphorylated p38 mitogen activated protein kinase (p38 MAPK), -$p21^{Cip1}$, -$p27^{kip1}$ and -cdk4 antibodies were purchased from Affinity BioReagents (Golden, CO). Anti-RhoA antibodies were purchased from Cell Signaling Technology (Danvers, MA). Anti-myelin basic protein (MBP, clone 1: 129-138), -proteolipid (PLP), -adenomatus polyposis coli (APC), -olig2, and -A2B5 antibodies were purchased from Serotec (Raleigh, NC). Mouse IgG and rabbit polyclonal IgG (control primary antibodies) and secondary antibodies such as Texas red-X-conjugated goat anti-mouse IgG and fluorescein (FITC)-conjugated goat anti-rabbit IgG were from Vector Laboratory (Burlingame, CA). [1(n)-^{3}H] GGPP, triammonium salt (1.85MBq), ECL-detecting reagents and nitrocellulose membranes were purchased from Perkin Elmer (California USA).

Cultures and treatments of OPCs

Mixed glial cell cultures were generated from P1–P2 Sprague Dawley rat brains (Charles River, Wilmington, MA) as described earlier (McCarthy and de Vellis 1980). Briefly, dissociated cortices were cultured on poly-lysine coated cultures flasks in DMEM containing 10% FBS and 4 mM L-glutamine. After 10 days, flasks were shaken at 250 rev/min for 2 h to remove microglia. Then, flasks were shaken for another 8h in which OPCs were dislodged from the astrocyte layer and re-plated on laminin-2 coated culture dishes or glass cover slips in high-glucose, Sato-based medium containing 5 μg/ml insulin, 50 μg/ml human transferrin, 100 μg/ml BSA, 6.2 μg/ml progesterone, 16 μg/ml putrescine, 5 ng/ml sodium selenite and 4 mM L-glutamine. Purity of OPCs as 90% was confirmed by staining with anti-A2B5 antibodies. OPCs were cultured in dishes or on glass cover slips (2,000 cells/cm^2) for 24 hr in Sato medium supplemented with recombinant platelet derived growth factor-AA and fibroblast growth factor-2 proteins 10 ng/ml each. After 24 h, fresh Sato medium supplemented with 2% FBS and 10 ng/ml of recombinant ciliary neurotrophic factor protein was added. Treatment with LOV or other agents was started on the same day. Rat OL-like B12 cells (gift from D. Schubert from the Salk Institute, La Jolla, CA) were preferred for transfection studies as they are well characterized and express OL proteins upon differentiation (Roth et al. 2003). Moreover, B12 cells demonstrated better transfection efficiency in our hands than primary OPCs. B12 cells were plated at 10^5 cells/ml in Dulbecco's modified Eagle medium (DMEM) containing 5% FBS and 25 μg/ml gentamycin in 25-cm^2 flasks (Nunc, Roskilde, Denmark) and incubated at 37 °C in a humidified atmosphere of 95% air and 5% CO_2 (Calderon et al. 1998). Media was replaced with drug-containing media 24 h after plating and every 12 h thereafter.

Flow cytometry (FACS) analysis

Cells were washed and re-suspended in PBS containing 3% BSA and incubated with 10 μg/mlnon-immune mouse IgG for 15 min. After washing, cells were incubated with 2 μg/ml of appropriate antibodies diluted 1:100 in PBS containing 3% BSA at 4 °C for 30 min. After washing, cells were incubated at 4 °C for 30 min with PE-conjugated goat anti-rabbit IgG or FITC-conjugated goat anti-mouse IgM diluted at 1:200 and measured in an FL-1 channel (530±15 nm band pass filter). Cells were washed before analysis on a FACScalibur flow cytometer (BD Biosciences) operating with the Cell Quest^{TM} software. Dead cells and debris were excluded from the analysis by gating living cells from size/structure density plots. Data were displayed on a logarithmic scale with increasing fluorescence intensity (not shown). Histogram plot was recorded for at least 10,000gated events and the percentage of positive cells was plotted.

Collection of cellular cytosolic and membranal fractions

Membranal and cytosolic fractions of treated cells were collected as described earlier (Paintlia et al. 2008). Cytosolic and membranal fractions were subjected to determine the distribution of RhoA by western blotting or by using an ELISA-based kit as described in the product manual (Cytoskeleton, Inc.). RhoA activity was plotted as the membranal vs. cytosolic ratio.

SREBP-2 transcription factor assay kit

SREBP-2 transcription factor activity was detected in the nuclear extract of treated cells per manufacturer instructions (Cayman Chemicals, Ann Arbor Michigan).

Metabolic labeling

De novo incorporation of GGPP into cell proteins was assessed using a procedure described earlier (Dunn et al. 2006). In brief, cells were cultured and treated in 100-mm plates. After 24 h, cells were pulsed with [1(n)-^{3}H]-GGPP ammonium salt (20 μCi) and cultured for additional 24 h followed by harvesting, sonication, SDS-PAGE, and autoradiography.

Immunocytochemistry/immunohistochemistry

Cells/tissue sections on slides were blocked with a serum-PBS solution and incubated with appropriately diluted primary antibodies at 4 °C overnight followed by washing and incubation with secondary antibodies. For double-labeling primary, antibodies were added separately after the completion of labeling for one marker. Slides were also incubated with Texas red-conjugated IgM without primary antibody as negative controls and an appropriate mouse IgG and rabbit polyclonal IgG were used as isotype controls. After thorough washings, slides were mounted with aqueous mounting media (Vectashield, Vector Labs; Burlingame, CA). Slides were analyzed by immunofluorescence microscopy (Olympus BX-60) with an Olympus digital camera (Optronics; Goleta, CA). Images were captured and processed using Adobe Photoshop 7.0 software.

The length of OL processes was determined by photographing random fields of cells with phase contrast microscope at an amplification of x100 using IMAGE pro 4.0 software (Media Cybernetics, Silver Spring, MD). 20–60 cells/photograph were measured and analyzed by comparing cell process length to major cell body diameter as described earlier (Riboni et al. 1995). OLs labeled with anti-APC antibodies were counted manually in the brain or spinal cord (SC) tissue sections. For detection of RhoA activation in treated cells, glass slides were permeabilized and incubated with GST tagged rhotekin binding domain (RBD), which binds to GTP-RhoA (active form) and detected with anti-GST antibodies along with cell specific marker antibodies by standard methods and photographed as

described above. Histological examination and immunohistochemistry of tissue sections prepared by using standard methods were stained with Luxol fast blue (LFB) dye or with MBP and PLP antibodies to analyze myelin integrity. Then sections were photographed using light microscopy (Olympus BX-60) with an Olympus digital camera as described above.

RNA preparation, cDNA synthesis and quantitative real-time PCR analysis

Cells or tissues were carefully processed for RNA isolation using TRIZOL reagent followed by cDNA synthesis and real-time PCR analysis using iCycler iQ Real-Time PCR Detection System (BIO-RAD Laboratories) as described previously (Paintlia et al. 2005). Primer sets used in the study (Table 1) were designed and purchased from Integrated DNA Technologies (Coralville, IA, USA). IQ^{TM} SYBR Green Supermix was purchased from BIO-RAD (Hercules CA). Thermal cycling conditions were as follows: activation of iTaq^{TM} DNA polymerase at 95 °C for 10 min, followed by 35 cycles of amplification at 95 °C for 30 s and 55–57.5 °C for 1 min. The specificity and detection methods for data analysis are as described earlier (Paintlia et al. 2008). In brief, real-time PCR specificity for each analysis was determined by melting curve analysis of amplified product. Normalized expression of target gene was calculated with the expression of reference gene (18S rRNA or GAPDH). The detection threshold was set above the mean baseline fluorescence determined by the first 20 cycles. A standard curve for each template was generated using a serial dilution of the template (cDNA).

Western blot and immunoblotting

Cells or tissues were processed in ice-cold lysis buffer followed by Western blot analysis as described previously (Paintlia et al. 2005).

Transfection Studies

Lipofectamine was used for transfection of cells according to the manufacturer's instructions. Briefly, 5,000 cells/cm^2 were plated onto each plate of a 6-well multiplate and cultured for 24 hr in DMEM with 5% FBS. A total of 1–3 μg of RhoA dominant negative (dn) and RhoA constitutively active (ca) expression vectors along with 0.3 μg of ptk-PPRE3-*luc* (kind gift of Dr. R. Evans, Salk Institute, La Jolla) or 50 ng of constitutive β-galactosidase expression vector (pCMV-*βgal*; Clonetech, CA) were used for transfection studies. Similarly, cells were transiently transfected with 0.3 μg of pMBP-P6L3-*luc* (kind gift from Dr. R. Miskimins, University of South Dakota, Vermillion, SD) or 50 ng of constitutive β-galactosidase expression vector (pCMV-*βgal*; Clonetech, CA). After 24 h of transfection, cells were treated with compounds for the next 24 h and reporter (luciferase) activity was measured with a Luciferase Assay kit (Promega, Madison, WI USA) and normalized against β-galactosidase (Invitrogen, Carlsbad, CA). Likewise, 1–3 μg of each pAkt-*ca*, pPTEN-*dn*, pAkt-*dn* and pPTEN-*wt* plasmids or insert less pcDNA3 plasmids were used for transfection of B12 cells. After 24 h, cells were treated with compounds and analyzed by proliferation assay as described below. TriEFCTa kits for small interfering RNAs (siRNA) for PPAR-γ and PTEN oligonucleotides kits were purchased from IDT DNA Technologies Inc (San Diego, California) for knock down of PPAR-γ and PTEN expression in cells as described in the product manual.

Proliferation assay

[^{3}H]-thymidine DNA incorporation was measured in cells by a 1450 Microbeta Wallac Trilux Liquid Scintillation Counter (Perkin-Elmer Life Sciences) using procedures described previously (Nath et al. 2004).

Cholesterol extraction and amplex red assay

Cells (10^4–10^5) or homogenized tissues were suspended in isopropanol (500 μl) and ssonicated with a microprobe for 10s. After centrifugation, supernatant was used for cholesterol analysis using Amplex Red Cholesterol Assay kit (Invitrogen, Carlsbad, CA). The pellet was suspended in 0.1 M sodium hydroxide (100 ml) and protein was measured. Similarly, total cholesterol was measured directly in serum samples.

Detection of cytotoxicity

Cytotoxicity of pharmacological agents in treated cells was detected by using LDH release assay kit (Roche Diagnostics, Indianapolis, IN).

Treatment of animals with LOV

Normal female Lewis rats (n=6 each group) were treated with LOV (2 or 5 mg/kg; ip) daily for 6 months to determine the effect of LOV in the CNS of normal rats. After 6 months, rats were sacrificed to collect their blood, spinal cords, and brain samples.

Statistical analysis

With Student's unpaired t-test and one-way multiple range ANOVA (Student-Newman-Keuls — compare all column pairs), *p* values were determined for respective experiments from 3 identical experiments using GraphPad Prism 3.0 software (GraphPad Software Inc. San Diego, CA). The criterion for statistical significance was <0.05.

RESULTS

Depletion of intracellular cholesterol is critical to OPCs

Cholesterol homeostasis in the cell is maintained via biosynthesis of cholesterol and/or low density lipid receptor (LDLR)-mediated uptake of exogenous cholesterol (Brown and Goldstein 1979; Smith et al. 1990). Because recent studies reported that statin treatment impedes OL differentiation *in vitro* (Klopfleisch et al. 2008; Maier et al. 2008), we investigated whether this effect of statin on OPCs is attributed to the depletion of intracellular cholesterol. Fig. 1 depicts the metabolites and inhibitors of mevalonate-pathway used in the study. Primary OPCs were treated with LOV in cholesterol- or FBS-deprived culture conditions to determine the transcriptional activity of sterol-responsive element-binding protein (SREBP)-2 and expression of LDLR. The expression of LDLR is regulated by SREBP-2 activation (Ma et al. 2008). Interestingly, LOV enhanced SREBP-2 activity in OPCs cultured in serum-deprived media, which diminished significantly in the presence of 2% FBS or 10 μM of cholesterol (Fig. 2A). Moreover, the smaller inhibition of SREBP-2 activity in LOV-treated OPCs in the presence of <2% FBS was improved by supplementation of cholesterol (Fig. 2A). Likewise, LDLR expression was greater in LOV-treated OPCs in serum-deprived cultures, which was reversed in the presence of cholesterol or FBS in a concentration-dependent manner (Fig. 2B). Correspondingly, a significant reduction of cellular cholesterol was observed in LOV-treated OPCs under cholesterol-deprived conditions compared to controls, which was reversed in the presence of FBS (concentration-dependent manner) or cholesterol (Fig. 2C). Moreover, LOV caused cell death (≈75%) of OPCs under cholesterol deprived culture conditions (Fig. 2D), which was abolished in the presence of cholesterol or FBS (2%). Of note, FBS concentration ≤1% was not sufficient to prevent the detrimental effect of LOV on OPCs. The observed increase in the expression of LDLR with parallel decrease in the level of cellular cholesterol in LOV treated OPCs under cholesterol/FBS deprived conditions and its normalization by supplementation of FBS (2%)/cholesterol suggesting that cholesterol homeostasis (Fig. 2C) is important to maintain cellular integrity (Fig. 2D) via LDLR mediated uptake of

extracellular cholesterol during statin treatment. In addition, these data provide evidence that statin-mediated depletion of intracellular cholesterol was responsible for impeded differentiation of OLs *in vitro* under cholesterol/serum-deprived culture conditions as non-physiological conditions used previously (Klopfleisch et al. 2008; Maier et al. 2008). Thus, for subsequent studies we opted to use 2% FBS in OPC cultures.

Decrease in mevalonate – pathway metabolite (s) is involved in the differentiation of OPCs

Previously, we documented that LOV enhances the differentiation of OPCs in serum-deprived mixed glial cultures (Paintlia et al. 2005; Paintlia et al. 2008). Here, we investigated whether LOV mimics similar in cultures enriched with 2% FBS. As expected, LOV significantly promoted the development of OPCs into premyelinating OLs: the percentage of $O1^+$ (marker associated with postmitotic commitment and initiation of terminal differentiation of OLs) increased compared with controls (Fig. 3A). This effect of LOV on OPCs was reversed in the presence of mevalonate (Fig. 3A), suggesting that involvement of mevalonate-pathway. Phase-contrast microscopy and immunocytochemistry corroborated these data (Fig. 3B) and demonstrated a significant ($p<0.05$) increase in the percentage of $O1^+$ phenotype cells (22 ± 3) in OPCs treated with LOV versus untreated cells (10 ± 2). The observed increase in cell density of LOV-treated OPCs compared to untreated ones on cover slips could be due to an increase in the survival of differentiating OLs (Fig. 3B). This increase in cell density was associated with significant increases in the extension of OL processes in LOV-treated cells compared to controls (Fig. 3C). The observed phenotypic changes in LOV-treated OPCs were corroborated by significant increases in MBP expression and decreases in PDGF-αR expression (Fig. 3D-E), indicating the commitment of OPCs to a differentiation program. It was supported by increase in the level of MBP protein in differentiated OLs. These data imply that serum enrichment mimic the effect of LOV on OPCs in serum-deprived mixed-glial cultures (Paintlia et al. 2005; Paintlia et al. 2008) thereby demonstrating the significance of cholesterol homeostasis in the survival and differentiation of OPCs during statin treatment.

GGPP depletion mediated inhibition of RhoA-ROCK signaling in OPCs

Previous studies indicated that statin-mediated regulation of RhoA activity is involved in OPC differentiation in purified or mixed glial cultures (Miron et al. 2007; Paintlia et al. 2008). Therefore, we next investigated whether same mechanism is responsible for OPC differentiation with LOV treatment in FBS (2%)-enriched cultures. OPCs were treated with LOV in the presence/absence of various metabolites or inhibitors of the mevalonate-pathway including inhibitors of RhoA and ROCK (Fig. 1). As expected, FACS analysis demonstrated a significant increase in the percentage of MBP^+ cells in LOV treated purified OPC cultures compared to controls, which was blocked in the presence of mevalonate/GGPP, but not FPP (Fig. 3F). The effect of LOV on OPCs was mimicked by treatment with inhibitors of geranylgeranyl transferase (GGTI-298), ROCK (Y27632) and Rho family GTPases (C3-exoenzyme), but not with farnesyl transferase (FTI-277) (Fig. 3F). Likewise, LOV-mediated increases in MBP and SOX10 (OL transcription factor) transcripts in treated OPCs was inhibited in the presence of GGPP, but this effect of LOV was mimicked by GGTI-298 or Y27632 (Fig. 3G-H). These data suggest that GGPP depletion is involved in the inhibition of RhoA-ROCK signaling in LOV treated OPCs. The observed inhibition of RhoA in LOV-treated OPCs was further corroborated by i) dose-dependent reductions in RhoA protein in the membranal fractions versus cytosolic fractions of LOV-treated OPCs (Fig. 4A), ii) reduced active RhoA in MBP expressing OLs versus LOV-treated OPCs (Fig. 4B) and iii) reduced phosphorylated cofilin, a down-stream target of RhoA, in LOV-treated OPCs (Fig. 4A).

To establish the involvement of GGPP depletion in an inhibition of RhoA in LOV treated OPCs, we treated OPCs with squalene synthase inhibitor (ZAA; zaragozic acid A). ZAA is known to block the biosynthesis of intracellular cholesterol, but not isoprenoids (Fig. 1). Interestingly, ZAA exposure significantly blocked the differentiation of OPCs into myelin-forming OLs as shown by significant decreases in the percentage of MBP^+ cells compared with controls (Fig. 4C). However, a significant increase in the percentage of $NG2^+$ (proliferating OPC marker) and $O4^+$ (late-OPCs) cells was observed by ZAA treatment as compared to controls (Fig. 4C). This effect of ZAA on OPCs was not reversed in the presence of exogenous cholesterol (Fig. 4C), suggesting that an accumulation of isoprenoids increases the pool of active small GTPases including RhoA in OPCs leading to their increased proliferation instead of differentiation. These conclusions were corroborated by dose-dependent increases in the *de novo* synthesis of proteins labeled with [1(n)-^{3}H] GGPP (Fig. 4D) and increased RhoA activity in a dose-dependent manner (Fig. 4E) in OPCs treated with ZAA. These data provide evidence that GGPP depletion inhibits RhoA-ROCK signaling, which participates in the differentiation of LOV treated OPCs.

Transcriptional activation and expression of PPAR-γ in LOV treated OPCs

Previous studies indicated that RhoA and PPAR-γ have an inverse relationship in statin-treated OPCs (Miron et al. 2007; Sim et al. 2008); however, the mechanism for this relationship is unknown. Thus, we next investigated whether LOV-mediated inhibition of RhoA-ROCK signaling participates in the regulation of PPAR-γ activities in OPCs. Western blot analysis revealed a dose-dependent increase in PPAR-γ protein in LOV-treated OPCs (Fig. 5A). Correspondingly, PPAR-γ transcripts were also significantly increased in LOV-treated OPCs compared to controls, which was reversed by mevalonate or GGPP, but not by FPP (Fig. 5B). Again, this effect of LOV in OPCs was mimicked by GGTI-298, C3-exoenzyme and Y27632, but not by FTI-277 (Fig. 5B), suggesting that an inhibition of RhoA signaling induces PPAR-γ expression in LOV treated OPCs.

PPAR-γ activation was also increased in LOV-treated OPCs as demonstrated by significant increases in nuclear translocation of PPAR-γ protein from the cytosol to controls (Fig. 5C). Similar observation was made by treatment with PPAR-γ agonist, ciglitazone (CGN) as positive control (Fig. 5C). To confirm RhoA inhibition mediated PPAR-γ activation in LOV treated OPCs, we transiently transfected B12 cells with ptk-PPRE-*luc* (reporter plasmids) and RhoA-dominant negative (dn)/or -constitutively active (ca) plasmids including siRNAs of PPAR-γ. LOV induced significant increases in reporter activity in B12 cells transfected with ptk-PPRE-*luc* plasmids compared with controls (Fig. 5D). Similar observation was made in B12 cells co-transfected with ptk-PPRE-*luc* and pRhoA-*dn* plasmids (Fig. 5D). The observed effect of LOV in B12 cells transfected with ptk-PPRE-*luc* was abolished by co-transfection with PPAR-γ siRNAs or in the presence of GW9662, antagonist of PPAR-γ (Fig. 5D). Importantly, LOV-induced effects in B12 cells transfected with ptk-PPRE-*luc* were mimicked by GGTI-298 and Y27632 including CGN and 15d-PGJ2, as PPAR-γ agonists (Fig. 5D), suggesting that LOV-mediated inhibition of RhoA-ROCK signaling is involved in the transcriptional activation of PPAR-γ in OPCs. Of note, no induction of luciferase activity was observed in B12 cells co-transfected with ptk-PPRE-*luc* and pcDNA3 (without insert) plasmids or/with ptk-PPRE-*luc* and pRhoA-*ca* plasmids (Fig. 5D).

Next, to assess whether this LOV-mediated activation of PPAR-γ is associated with an increase in the bio-availability of its endogenous activators i.e., 15d-PGJ2 in OPCs, we measured the expression of enzymes involved in the biosynthesis of these activators. Interestingly, a significant dose-dependent increases in the mRNAs of $cPLA_2$ (Fig. 5E) and COX-2 (Fig. 5F) including the protein of COX-2 (Fig. 5G) were observed in OPCs treated with LOV compared to controls. Together, these data imply that the observed activation and

induction of PPAR-γ expression in LOV-treated OPCs are attributed to an inhibition of RhoA-ROCK signaling.

Induction of PTEN and its effect on the proliferation of LOV treated OPCs

Previously, LOV was described to inhibit the proliferation of cancer cells via PPAR-γ-mediated induction of PTEN (Teresi et al. 2006). Therefore, we next investigated whether LOV induces PTEN expression in treated OPCs. Interestingly, LOV significantly enhanced the expression of PTEN in treated OPCs compared with controls (Fig. 6A). This effect of LOV was reversed in the presence of GGPP or GW9662 (PPAR-γ antagonist), but not with FPP (Fig. 6A), suggesting that LOV-mediated PPAR-γ activation is involved an induction of PTEN expression in OPCs. Western analysis corroborated these data and demonstrated a dose-dependent increase in PTEN protein (Fig. 6B), including its phosphorylation (important for PTEN stability) (Fig. 6C) in LOV-treated OPCs compared with controls. Because PTEN is known to inhibit cell proliferation via inhibition of PI3K-Akt signaling (Salmena et al. 2008; Sun et al. 1999), we next analyzed the activation status of this signaling pathway in treated OPCs with LOV or CGN. As shown in Fig. 6D, LOV inhibited the phosphorylation of Akt in treated OPCs, supporting the involvement of PTEN to inhibit proliferation of LOV treated OPCs. Moreover, the observed increased phosphorylation of both p38 MAPK and ERKs (44/42) in LOV-treated OPCs (Fig. 6D) supported the differentiation and survival of OLs. Similar observation was made by treatment with CGN (Fig. 6C-D) suggesting that LOV-mediated PPAR-γ activation induces PTEN, which in turn accelerate the differentiation of OPCs.

To further establish the participation of PTEN in an inhibition of OPC proliferation, we treated B12 cells with various pharmacological agents or transfected them with recombinant plasmids or PTEN siRNA followed by analysis for [H^3] thymidine incorporation. LOV significantly inhibited the proliferation of treated B12 cells compared to controls, which was reversed in the presence of GW9662 (Fig. 7A). This effect of LOV in B12 cells was mimicked by treatment with CGN or specific inhibitors of PI3K (wortmannin) and Akt (Akt inhibitor) (Fig. 7A). Moreover, LOV- and CGN-induced effects in B12 cells were abolished by transient transfection with PTEN siRNAs (Fig. 7A), thus corroborating the participation of PTEN in an inhibition of OPCs proliferation. Furthermore, LOV- and CGN-induced effects in B12 cells transfected with pcDNA3 plasmids were mimicked by transfection of B12 cells with pAkt-*dn* or pPTEN-*wt* plasmids individually (Fig. 7B), but reversed by transfection with pAkt-*ca* and/or pPTEN-*dn* plasmids, individually (Fig. 7B). No cell death was observed in B12 cells upon treatment with these pharmacological and biological agents (data not shown). Together, these data imply that LOV-mediated activation of PPAR-γ and PTEN signaling cascade inhibits the proliferation of OPCs via inhibition of PI3K-Akt signaling.

PPAR-γ and PTEN cascade induces cell cycle arrest in OPCs

Next we investigated whether LOV-mediated inhibition of proliferation leads to cell cycle arrest in OPCs, which is essential for their differentiation. Interestingly, a significant increase in of $p21^{Cip1}$ and $p27^{Kip1}$ transcripts with corresponding decrease in cdk4 transcripts were observed in LOV-treated OPCs compared to untreated controls (Fig. 8A). The effect of LOV in OPCs was mimicked by treatment with Y27632 or CGN (Fig. 8A). Western analysis showed a dose-dependent increase in $p21^{Cip1}$ and $p27^{Kip1}$ protein with a corresponding decrease in cdk4 protein in LOV-treated OPCs (Fig. 8B). There was significant increase in the percentage of $p21^{Cip1+}$ cells with a corresponding decrease in the percentage of $cdk4^{+}$ cells in LOV-treated OPCs compared to controls, which was reversed by mevalonate co-treatment (Fig. 8C), suggesting that LOV induces cell cycle arrest at G1 phase in treated OPCs.

Because $p27^{Kip1}$ is reported to regulate the expression of MBP during cell cycle exit in OPCs (Wei et al. 2003; Wei et al. 2004), we next investigated whether LOV-mediated induction of $p27^{Kip1}$ induces MBP promotor activity in treated OPCs. LOV significantly increased luciferase activity in B12 cells transiently transfected with pMBP-P6L3-*luc* (plasmid with inserted MBP promotor sequence) compared to controls (Fig. 8D). This effect of LOV in B12 cells was mimicked by treatment with GGTI-298, Y27632 and CGN, but reversed by PPAR-γ antagonist, GW9662 or co-transfection with siRNAs of PPAR-γ or PTEN (Fig. 8D), suggesting that RhoA-ROCK mediated activation of PPAR-γ and PTEN cascade induces cell cycle arrest in LOV-treated OPCs.

Finally, to confirm whether PPAR-γ and PTEN signaling is directly involved in the differentiation of OPCs, we transfected OPCs with siRNAs of PPAR-γ or PTEN individually and treated with LOV. The observed LOV-mediated increase in expression of MBP and SOX10 (a transcription factor) in primary OPCs transfected with scramble siRNAs was reversed significantly in those OPCs transiently transfected with siRNAs of PPAR-γ or PTEN (Fig. 8E-F). Together, these data imply that activation of PPAR-γ and PTEN cascade is involved in the differentiation of LOV treated OPCs.

Evaluation of the CNS of LOV treated normal rats

We next investigated whether the observed effect of LOV on OPCs *in vitro* can deplete their pool in the brain parenchyma of treated normal individuals. To address this, female Lewis rats were treated with LOV (2 or 5 mg/kg; ip) daily for 6 months. LOV dose was selected based upon its protective activities in an EAE model (Nath et al. 2004; Paintlia et al. 2008). We observed no change in the behavior of animals or in the level of PDGF-αR and Olig2 (marker for OPCs) or MBP (marker for matured OLs) mRNAs in the CNS of LOV-treated rats and controls (Fig. 9A-C). Similarly, cholesterol level was also unchanged in the CNS of LOV-treated rats compared with controls (Fig. 9D). As expected, serum cholesterol was reduced significantly ($p<0.03$) in normal rats treated with LOV (2 mg/kg, ip) i.e., 212 ± 21 (mg/L) versus controls treated with vehicle i.e., 345 ± 33 (mg/L). These observations document that the dose of LOV, which attenuates EAE (Nath et al. 2004; Paintlia et al. 2008) decreases the level of cholesterol in the serum, but not in the CNS of EAE (Paintlia et al. 2005) or control rats (Fig. 9D).

Histological examination using LFB staining revealed no change in the myelin integrity in the corpus-callosum of the brain and in the dorsal funiculi of the SC of rats treated with LOV versus controls (Fig. 10A). Immunohistochemistry studies further demonstrated that the distribution of MBP and PLP in the myelin sheath was normal in the white matter i.e., corpus-callosum including cingulum of the brain and the dorsolateral funiculi of the SC of rats treated with LOV compared with controls (Fig. 10B). Likewise, no change in the level of Olig2, MBP, PTEN and PPAR-γ protein was observed in the SC of rats treated with LOV versus controls (Fig. 10C). The count of APC^{+} cells as marker of matured OLs was also unchanged in the brain (CON; 46 ± 3 vs. LOV; 48 ± 5) and SC (CON; 21 ± 2 vs. LOV; 24 ± 4) of rats (Fig. 10D). Together, these data imply that LOV concentrations that attenuates EAE and promote remyelination does not alter the pool of OPCs, myelin integrity and cholesterol in the CNS of normal rats thereby indicating that statins are therapeutically safe in humans to use for long-time.

DISCUSSION

Cholesterol homeostasis is essential for the survival of LOV treated OPCs

In contrast to previous studies (Miron et al. 2007; Paintlia et al. 2005; Paintlia et al. 2008; Sim et al. 2008), statins are reported to have negative impact on the differentiation of OLs *in*

vitro (Klopfleisch et al. 2008; Maier et al. 2008). Clearly, tissue culture conditions in these conflicting studies (deprived of cholesterol/serum) were totally different, and pig cells were used in one of the studies. Herein, we attempted to address the cause of impeded differentiation of OLs by statins *in vitro* settings. Statin (HMG-CoA reductase inhibitor) depletes cholesterol and isoprenoids in the cells (Fig. 1). Our studies conducted in cholesterol/FBS-deprived cultures established that LOV-mediated depletion of intracellular cholesterol was detrimental to OPCs as it was abolished by enrichment of cultures with FBS (2%) or cholesterol. Consistent with this, simvastatin-mediated retraction of OL processes has previously been reported to be rescued by cholesterol or isoprenoid co-treatment (Miron et al. 2007). Moreover, simvastatin was reported to protect myelin and OLs against lysophosphatidyl choline induced toxicity in brain spheroid cultures enriched with 10% serum (Vereyken et al. 2009). Our studies provide evidence that the presence of serum in OPC cultures may mimic more closely *in vivo* conditions like those of mixed glial cultures (Paintlia et al. 2005), where astrocytes may benefit the survival and differentiation of OLs as they are reported to support neuron growth *in vivo* (Nieweg et al. 2009). Importantly, in contrast to previous reports (Maier et al. 2009), we demonstrated that the transport/distribution of MBP in OL processes was not affected by LOV in the presence of FBS *in vitro* as well as *in vivo* thereby demonstrating the importance of cholesterol homeostasis for OL survival.

GGPP-depletion mediated inhibition of RhoA-ROCK accelerates OPC differentiation

In agreement with previous reports (Miron et al. 2007; Sim et al. 2008), LOV enhanced the phenotypic commitment and differentiation of primary OPCs *in vitro*. This was attributed to the depletion of RhoA-ROCK inhibition (Miron et al. 2007; Paintlia et al. 2008) via depletion of GGPP in OPCs (Figs. 3 & 4). GGPP depletion inhibits the attachment of active RhoA to the membrane resulting in cytosolic accumulation, which inhibits down-stream cellular signaling (Cordle et al. 2005). Conversely, the accumulation of GGPP increases the level of active RhoA in OPCs leading to their increased proliferation (Fig. 4C-E). Active RhoA is known to regulate the cytoskeletal re-arrangement via LIM kinase-mediated phosphorylation of cofilin (Sumi et al. 2001). Cofilin is an actin-binding protein and its phosphorylation leads to the polymerization of actin filaments and formation of stress-fibers (Marcoux and Vuori 2005). We observed an increase in the extension of processes in OLs (Fig. 3C) with corresponding reduction of phosphorylated cofilin upon treatment with LOV (Fig. 4A) suggesting that RhoA inactivation regulates cytoskeletal dynamics and process extension in OPCs via inhibition of stress-fiber formation.

PPAR-γ and PTEN signaling cascade participates in OPC differentiation

Recent studies documented that PPAR-γ activation is important for the survival and terminal differentiation of OLs *in vitro* (Roth et al. 2003) as well as under inflammatory disease conditions (Paintlia et al. 2006). PPAR-γ activation demonstrated inverse relationship with RhoA inactivation in LOV treated OPCs (Fig. 5). This effect of LOV was accompanied with an increase in the expression of cPLA2 and COX-2 (Fig. 5E-G). COX-2 is involved in the production of prostaglandins including 15d-PGJ2 from arachidonic acid as observed in statin-treated cells (Smith et al. 2002; Smith et al. 2005). Our data imply that LOV increases the bioavailability of PPAR-γ activators in treated OPCs via activation of cPLA2 and COX-2. In addition, the activation of p38 MAPK has been shown to play role in OL differentiation (Hamanoue et al. 2007) and its activation is reported to regulate COX-2 expression in epithelial cells (Shafer and Slice 2005). Therefore, the observed increase in p38 MAPK in LOV-treated OPCs further indicates that an activation of PPAR-γ is associated with p38-MAPK-mediated induction of COX-2 (Fig. 5F-G). The expression of PPAR-γ was reported to be induced in the presence of specific activators in different cell types (Bernardo et al. 2000). Thus, we observed an increase in the expression of PPAR-γ in

LOV-treated OPCs (Fig 5A-B), suggesting a positive feedback loop may exist in OPCs by which activators could sustain the responsiveness of these cells via increasing the expression of their cognate receptors.

Earlier, PPAR-γ was reported to induce PTEN expression in statin-treated non-neuronal cells (Teresi et al. 2006; Zhang et al. 2006). PTEN plays important role to induce cell cycle arrest in cancer cells via inhibition of PI3K-Akt signaling (Sun et al. 1999). Also, PTEN is reported to regulate neuronal differentiation (Lachyankar et al. 2000) and its deficiency in the brain causes defects in synaptic structure and myelination abnormalities (Fraser et al. 2008). Our findings demonstrated that PTEN participates in the differentiation of LOV treated OPCs ascribed to an activation of PPAR-γ and inhibition of PI3K-Akt signaling via inhibition of RhoA-ROCK (Fig. 6). Conversely, activation of PI3K-Akt signaling is reported to be essential for the survival and differentiation of OLs (Shankar et al. 2003). Differently, we observed an activation of ERKs (44/42) as an alternate survival signaling in LOV treated OPCs (Fig. 6D). These data are in agreement with observed opposing activation of ERKs (44/42) and Akt pathways in differentiating Schwann cells (Ogata et al. 2004).

Supporting an induction of cell cycle arrest at G1 phase in OPCs (Belachew et al. 2002; Ghiani et al. 1999), we observed an increase in the level of $p21^{Cip1}$ and $p27^{Kip1}$ with a corresponding reduction of cdk4 in LOV-treated OPCs (Fig. 8A-C), which was again attributed to an inhibition of RhoA-ROCK signaling in OPCs. RhoA has been reported to regulate G1/S cell cycle progression via down-regulation of $p21^{Cip1}$ and $p27^{kip1}$ (Croft and Olson 2006; Terano et al. 1998). In addition, $p27^{kip1}$ regulates the expression of MBP in OLs via activation of transcription factors i.e., Sp1 and SOX10 (Wei et al. 2003; Wei et al. 2004). In agreement with this, we observed an increased MBP promotor activity in LOV-treated B12 cells (Fig. 8D) expressions of MBP and $p27^{kip1}$ in LOV treated OPCs (Fig. 3E), suggesting that the expression of cell cycle inhibitors, in part, mediate the differentiation of LOV treated OPCs.

No effect on the pool of OPCs or myelin integrity in chronically treated rats with LOV

The observed enhanced differentiation of OPCs by statins *in vitro* by others (Miron et al. 2007; Sim et al. 2008) and our data raised the possibility that statin may deplete the pool of OPCs in the brain parenchyma of treated individuals, which may affect the long-term regenerative competence of the adult white matter. In this context, chronically treated normal rats with optimal dose (s) of LOV tested in EAE models demonstrated no change in the pool of OPCs/cholesterol in the CNS (Fig. 9). In addition, myelin integrity and the distribution of MBP/PLP protein was intact in the white matter of CNS in chronically treated rats with LOV (Fig. 10). Likewise, no change in the myelin contents was observed in the CNS of normal rats treated with LOV for short period of 3 weeks (Paintlia et al. 2005), providing an evidence that chronic treatment with statins is therapeutically safe. However, these *in vivo* effects of LOV on OPC differentiation or induction of PPAR-γ and PTEN expressions were quite opposite to that was observed *in vitro*. Reasons for such differences could be due to the dilution of the message for these genes as a whole brain measurement *in vivo* versus purified OLs used *in vitro* or the controlled regulation of PPAR-γ expression in the normal brain. Moreover, we previously documented that LOV induced the expression of PPAR-γ (Paintlia et al. 2004) and remyelination (Paintlia et al. 2005) in the CNS of EAE animals. In contrast, simvastatin was shown to impede the remyelination process in a cuprizone-CNS demyelinating model (non-EAE model) (Klopfleisch et al. 2008; Miron et al. 2009). Reason for such discrepancies in these models is not understood at this moment. One obvious reason could be the non-inflammatory/inflammatory nature including the site of demyelination in the CNS i.e., brain versus SC in non-EAE and EAE models, respectively. In support to this, recent study demonstrated that simvastatin attenuates hypoxia-ischemia induced hypomyelination in neonatal rats (Li et al. 2010), suggesting that

statins provide protective effects in inflamed CNS. Secondly, it could be attributed to the CNS penetrance of statins, as simvastatin was found at 6-fold higher concentrations and reduced brain cholesterol in chronically treated rats as compared to LOV (Johnson-Anuna et al. 2005).

In summary, the present study explains the possible cause behind the negative effects of statins on OLs *in vitro*. An inhibition of mevalonate pathway by statin induces the activation of PPAR-γ and PTEN cascade in differentiating OPCs, which is independent of the lowering of cholesterol (Fig. 1). Understanding of the cellular signaling mechanisms in the differentiation of OPCs may suggest new therapeutic interventions to improve remyelination in CNS demyelinating diseases including MS. In addition, the data provide evidence that chronic use of statins is safe for humans to treat CNS demyelinating diseases.

Acknowledgments

This study was supported by grants from the NIH (NS-22576, NS-34741, NS-37766, NS-038236, C06-RR015455, and C06-RR018823. We thank Dr. Jennifer G. Schnellmann for critical reading of this manuscript and Ms. Joyce Brian and Ms. Carrie Barnes for their technical assistance.

ABBREVIATIONS USED

MS	multiple sclerosis
EAE	experimental autoimmune encephalomyelitis
OL	oligodendrocyte
OPC	oligodendrocyte progenitor cell
LOV	lovastatin
ROCK	RhoA kinase
CGN	ciglitazone
PPAR	peroxisomal proliferator activated receptor
PTEN	tumor suppressor phosphatase and tensin homolog
cdk	cyclin dependent kinase
GGPP	geranylgeranyl-pyrophosphate
FPP	farnesyl pyrophosphate
GGTI	geranylgeranyl transferase inhibitor
FTI	farnesyl transferase inhibitor
BBB	blood brain barrier
FBS	fetal bovine serum and ZAA, zaragozic acid A

BIBLIOGRAPHY

Back SA, Tuohy TM, Chen H, Wallingford N, Craig A, Struve J, Luo NL, Banine F, Liu Y, Chang A, et al. Hyaluronan accumulates in demyelinated lesions and inhibits oligodendrocyte progenitor maturation. Nat Med. 2005; 11(9):966–72. [PubMed: 16086023]

Baer AS, Syed YA, Kang SU, Mitteregger D, Vig R, Ffrench-Constant C, Franklin RJ, Altmann F, Lubec G, Kotter MR. Myelin-mediated inhibition of oligodendrocyte precursor differentiation can be overcome by pharmacological modulation of Fyn-RhoA and protein kinase C signalling. Brain. 2009; 132(Pt 2):465–81. [PubMed: 19208690]

Belachew S, Aguirre AA, Wang H, Vautier F, Yuan X, Anderson S, Kirby M, Gallo V. Cyclin-dependent kinase-2 controls oligodendrocyte progenitor cell cycle progression and is downregulated in adult oligodendrocyte progenitors. J Neurosci. 2002; 22(19):8553–62. [PubMed: 12351729]

Bernardo A, Levi G, Minghetti L. Role of the peroxisome proliferator-activated receptor-gamma (PPAR-gamma) and its natural ligand 15-deoxy-Delta12, 14-prostaglandin J2 in the regulation of microglial functions. Eur J Neurosci. 2000; 12(7):2215–23. [PubMed: 10947800]

Brown MS, Goldstein JL. Receptor-mediated endocytosis: insights from the lipoprotein receptor system. Proc Natl Acad Sci U S A. 1979; 76(7):3330–7. [PubMed: 226968]

Calderon FH, von Bernhardi R, De Ferrari G, Luza S, Aldunate R, Inestrosa NC. Toxic effects of acetylcholinesterase on neuronal and glial-like cells in vitro. Mol Psychiatry. 1998; 3(3):247–55. [PubMed: 9672900]

Chang A, Tourtellotte WW, Rudick R, Trapp BD. Premyelinating oligodendrocytes in chronic lesions of multiple sclerosis. N Engl J Med. 2002; 346(3):165–73. [PubMed: 11796850]

Charles P, Reynolds R, Seilhean D, Rougon G, Aigrot MS, Niezgoda A, Zalc B, Lubetzki C. Re-expression of PSA-NCAM by demyelinated axons: an inhibitor of remyelination in multiple sclerosis? Brain. 2002; 125(Pt 9):1972–9. [PubMed: 12183343]

Cordle A, Koenigsknecht-Talboo J, Wilkinson B, Limpert A, Landreth G. Mechanisms of statin-mediated inhibition of small G-protein function. J Biol Chem. 2005; 280(40):34202–9. [PubMed: 16085653]

Croft DR, Olson MF. The Rho GTPase effector ROCK regulates cyclin A, cyclin D1, and p27Kip1 levels by distinct mechanisms. Mol Cell Biol. 2006; 26(12):4612–27. [PubMed: 16738326]

Dawson MR, Levine JM, Reynolds R. NG2-expressing cells in the central nervous system: are they oligodendroglial progenitors? J Neurosci Res. 2000; 61(5):471–9. [PubMed: 10956416]

Dunn SE, Youssef S, Goldstein MJ, Prod'homme T, Weber MS, Zamvil SS, Steinman L. Isoprenoids determine Th1/Th2 fate in pathogenic T cells, providing a mechanism of modulation of autoimmunity by atorvastatin. J Exp Med. 2006; 203(2):401–12. [PubMed: 16476765]

Fraser MM, Bayazitov IT, Zakharenko SS, Baker SJ. Phosphatase and tensin homolog, deleted on chromosome 10 deficiency in brain causes defects in synaptic structure, transmission and plasticity, and myelination abnormalities. Neuroscience. 2008; 151(2):476–88. [PubMed: 18082964]

Ghiani CA, Yuan X, Eisen AM, Knutson PL, DePinho RA, McBain CJ, Gallo V. Voltage-activated K + channels and membrane depolarization regulate accumulation of the cyclin-dependent kinase inhibitors p27(Kip1) and p21(CIP1) in glial progenitor cells. J Neurosci. 1999; 19(13):5380–92. [PubMed: 10377348]

Hamanoue M, Sato K, Takamatsu K. Inhibition of p38 mitogen-activated protein kinase-induced apoptosis in cultured mature oligodendrocytes using SB202190 and SB203580. Neurochem Int. 2007; 51(1):16–24. [PubMed: 17459526]

Jeffery ND, Blakemore WF. Locomotor deficits induced by experimental spinal cord demyelination are abolished by spontaneous remyelination. Brain. 1997; 120 (Pt 1):27–37. [PubMed: 9055795]

Johnson-Anuna LN, Eckert GP, Keller JH, Igbavboa U, Franke C, Fechner T, Schubert-Zsilavecz M, Karas M, Muller WE, Wood WG. Chronic administration of statins alters multiple gene expression patterns in mouse cerebral cortex. J Pharmacol Exp Ther. 2005; 312(2):786–93. [PubMed: 15358814]

Klopfleisch S, Merkler D, Schmitz M, Kloppner S, Schedensack M, Jeserich G, Althaus HH, Bruck W. Negative impact of statins on oligodendrocytes and myelin formation in vitro and in vivo. J Neurosci. 2008; 28(50):13609–14. [PubMed: 19074034]

Kotter MR, Li WW, Zhao C, Franklin RJ. Myelin impairs CNS remyelination by inhibiting oligodendrocyte precursor cell differentiation. J Neurosci. 2006; 26(1):328–32. [PubMed: 16399703]

Lachyankar MB, Sultana N, Schonhoff CM, Mitra P, Poluha W, Lambert S, Quesenberry PJ, Litofsky NS, Recht LD, Nabi R, et al. A role for nuclear PTEN in neuronal differentiation. J Neurosci. 2000; 20(4):1404–13. [PubMed: 10662831]

Li A, Lv S, Yu Z, Zhang Y, Ma H, Zhao H, Piao H, Li S, Zhang N, Sun C. Simvastatin attenuates hypomyelination induced by hypoxia-ischemia in neonatal rats. Neurol Res. 2010

Ma KL, Ruan XZ, Powis SH, Chen Y, Moorhead JF, Varghese Z. Inflammatory stress exacerbates lipid accumulation in hepatic cells and fatty livers of apolipoprotein E knockout mice. Hepatology. 2008; 48(3):770–81. [PubMed: 18752326]

Maier O, De Jonge J, Nomden A, Hoekstra D, Baron W. Lovastatin induces the formation of abnormal myelin-like membrane sheets in primary oligodendrocytes. Glia. 2008; 57(4):402–413. [PubMed: 18814266]

Maier O, De Jonge J, Nomden A, Hoekstra D, Baron W. Lovastatin induces the formation of abnormal myelin-like membrane sheets in primary oligodendrocytes. Glia. 2009; 57(4):402–13. [PubMed: 18814266]

Marcoux N, Vuori K. EGF receptor activity is essential for adhesion-induced stress fiber formation and cofilin phosphorylation. Cell Signal. 2005; 17(11):1449–55. [PubMed: 16125057]

McCarthy KD, de Vellis J. Preparation of separate astroglial and oligodendroglial cell cultures from rat cerebral tissue. J Cell Biol. 1980; 85(3):890–902. [PubMed: 6248568]

Miron VE, Rajasekharan S, Jarjour AA, Zamvil SS, Kennedy TE, Antel JP. Simvastatin regulates oligodendroglial process dynamics and survival. Glia. 2007; 55(2):130–43. [PubMed: 17078030]

Miron VE, Zehntner SP, Kuhlmann T, Ludwin SK, Owens T, Kennedy TE, Bedell BJ, Antel JP. Statin therapy inhibits remyelination in the central nervous system. Am J Pathol. 2009; 174(5):1880–90. [PubMed: 19349355]

Nath N, Giri S, Prasad R, Singh AK, Singh I. Potential targets of 3-hydroxy-3-methylglutaryl coenzyme A reductase inhibitor for multiple sclerosis therapy. J Immunol. 2004; 172(2):1273–86. [PubMed: 14707106]

Nieweg K, Schaller H, Pfrieger FW. Marked differences in cholesterol synthesis between neurons and glial cells from postnatal rats. J Neurochem. 2009; 109(1):125–34. [PubMed: 19166509]

Ogata T, Iijima S, Hoshikawa S, Miura T, Yamamoto S, Oda H, Nakamura K, Tanaka S. Opposing extracellular signal-regulated kinase and Akt pathways control Schwann cell myelination. J Neurosci. 2004; 24(30):6724–32. [PubMed: 15282275]

Pahan K, Sheikh FG, Namboodiri AM, Singh I. Lovastatin and phenylacetate inhibit the induction of nitric oxide synthase and cytokines in rat primary astrocytes, microglia, and macrophages. J Clin Invest. 1997; 100(11):2671–9. [PubMed: 9389730]

Paintlia AS, Paintlia MK, Khan M, Vollmer T, Singh AK, Singh I. HMG-CoA reductase inhibitor augments survival and differentiation of oligodendrocyte progenitors in animal model of multiple sclerosis. Faseb J. 2005; 19(11):1407–21. [PubMed: 16126908]

Paintlia AS, Paintlia MK, Singh AK, Singh I. Inhibition of rho family functions by lovastatin promotes myelin repair in ameliorating experimental autoimmune encephalomyelitis. Mol Pharmacol. 2008; 73(5):1381–93. [PubMed: 18239032]

Paintlia AS, Paintlia MK, Singh AK, Stanislaus R, Gilg AG, Barbosa E, Singh I. Regulation of gene expression associated with acute experimental autoimmune encephalomyelitis by Lovastatin. J Neurosci Res. 2004; 77(1):63–81. [PubMed: 15197739]

Paintlia AS, Paintlia MK, Singh I, Singh AK. IL-4-induced peroxisome proliferator-activated receptor gamma activation inhibits NF-kappaB trans activation in central nervous system (CNS) glial cells and protects oligodendrocyte progenitors under neuroinflammatory disease conditions: implication for CNS-demyelinating diseases. J Immunol. 2006; 176(7):4385–98. [PubMed: 16547277]

Prineas JW, Barnard RO, Kwon EE, Sharer LR, Cho ES. Multiple sclerosis: remyelination of nascent lesions. Ann Neurol. 1993; 33(2):137–51. [PubMed: 8434875]

Riboni L, Prinetti A, Bassi R, Caminiti A, Tettamanti G. A mediator role of ceramide in the regulation of neuroblastoma Neuro2a cell differentiation. J Biol Chem. 1995; 270(45):26868–75. [PubMed: 7592930]

Roth AD, Leisewitz AV, Jung JE, Cassina P, Barbeito L, Inestrosa NC, Bronfman M. PPAR gamma activators induce growth arrest and process extension in B12 oligodendrocyte-like cells and terminal differentiation of cultured oligodendrocytes. J Neurosci Res. 2003; 72(4):425–35. [PubMed: 12704804]

Saher G, Brugger B, Lappe-Siefke C, Mobius W, Tozawa R, Wehr MC, Wieland F, Ishibashi S, Nave KA. High cholesterol level is essential for myelin membrane growth. Nat Neurosci. 2005; 8(4): 468–75. [PubMed: 15793579]

Salmena L, Carracedo A, Pandolfi PP. Tenets of PTEN tumor suppression. Cell. 2008; 133(3):403–14. [PubMed: 18455982]

Shafer LM, Slice LW. Anisomycin induces COX-2 mRNA expression through p38(MAPK) and CREB independent of small GTPases in intestinal epithelial cells. Biochim Biophys Acta. 2005; 1745(3):393–400. [PubMed: 16054711]

Shankar SL, O'Guin K, Cammer M, McMorris FA, Stitt TN, Basch RS, Varnum B, Shafit-Zagardo B. The growth arrest-specific gene product Gas6 promotes the survival of human oligodendrocytes via a phosphatidylinositol 3-kinase-dependent pathway. J Neurosci. 2003; 23(10):4208–18. [PubMed: 12764109]

Sim FJ, Lang JK, Ali TA, Roy NS, Vates GE, Pilcher WH, Goldman SA. Statin treatment of adult human glial progenitors induces PPAR gamma-mediated oligodendrocytic differentiation. Glia. 2008; 56(9):954–62. [PubMed: 18383345]

Smith JR, Osborne TF, Goldstein JL, Brown MS. Identification of nucleotides responsible for enhancer activity of sterol regulatory element in low density lipoprotein receptor gene. J Biol Chem. 1990; 265(4):2306–10. [PubMed: 2298751]

Smith LH, Boutaud O, Breyer M, Morrow JD, Oates JA, Vaughan DE. Cyclooxygenase-2-dependent prostacyclin formation is regulated by low density lipoprotein cholesterol in vitro. Arterioscler Thromb Vasc Biol. 2002; 22(6):983–8. [PubMed: 12067908]

Smith LH, Petrie MS, Morrow JD, Oates JA, Vaughan DE. The sterol response element binding protein regulates cyclooxygenase-2 gene expression in endothelial cells. J Lipid Res. 2005; 46(5): 862–71. [PubMed: 15716578]

Stanislaus R, Singh AK, Singh I. Lovastatin treatment decreases mononuclear cell infiltration into the CNS of Lewis rats with experimental allergic encephalomyelitis. J Neurosci Res. 2001; 66(2):155–62. [PubMed: 11592110]

Sumi T, Matsumoto K, Nakamura T. Specific activation of LIM kinase 2 via phosphorylation of threonine 505 by ROCK, a Rho-dependent protein kinase. J Biol Chem. 2001; 276(1):670–6. [PubMed: 11018042]

Sun H, Lesche R, Li DM, Liliental J, Zhang H, Gao J, Gavrilova N, Mueller B, Liu X, Wu H. PTEN modulates cell cycle progression and cell survival by regulating phosphatidylinositol 3,4,5,-trisphosphate and Akt/protein kinase B signaling pathway. Proc Natl Acad Sci U S A. 1999; 96(11):6199–204. [PubMed: 10339565]

Terano T, Shiina T, Noguchi Y, Tanaka T, Tatsuno I, Saito Y, Yasuda T, Kitagawa M, Hirai A. Geranylgeranylpyrophosphate plays a key role for the G1 to S transition in vascular smooth muscle cells. J Atheroscler Thromb. 1998; 5(1):1–6. [PubMed: 10077451]

Teresi RE, Shaiu CW, Chen CS, Chatterjee VK, Waite KA, Eng C. Increased PTEN expression due to transcriptional activation of PPARgamma by Lovastatin and Rosiglitazone. Int J Cancer. 2006; 118(10):2390–8. [PubMed: 16425225]

Vereyken EJ, Fluitsma DM, Bolijn MJ, Dijkstra CD, Teunissen CE. An in vitro model for de- and remyelination using lysophosphatidyl choline in rodent whole brain spheroid cultures. Glia. 2009; 57(12):1326–40. [PubMed: 19191324]

Wei Q, Miskimins WK, Miskimins R. The Sp1 family of transcription factors is involved in p27(Kip1)-mediated activation of myelin basic protein gene expression. Mol Cell Biol. 2003; 23(12):4035–45. [PubMed: 12773549]

Wei Q, Miskimins WK, Miskimins R. Sox10 acts as a tissue-specific transcription factor enhancing activation of the myelin basic protein gene promoter by p27Kip1 and Sp1. J Neurosci Res. 2004; 78(6):796–802. [PubMed: 15523643]

Youssef S, Stuve O, Patarroyo JC, Ruiz PJ, Radosevich JL, Hur EM, Bravo M, Mitchell DJ, Sobel RA, Steinman L, et al. The HMG-CoA reductase inhibitor, atorvastatin, promotes a Th2 bias and reverses paralysis in central nervous system autoimmune disease. Nature. 2002; 420(6911):78–84. [PubMed: 12422218]

Zhang W, Wu N, Li Z, Wang L, Jin J, Zha XL. PPARgamma activator rosiglitazone inhibits cell migration via upregulation of PTEN in human hepatocarcinoma cell line BEL-7404. Cancer Biol Ther. 2006; 5(8):1008–14. [PubMed: 16775433]

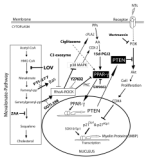

Fig. 1. Diagrammatic presentation of LOV-induced activation of PPAR-γ and PTEN cascade in OPCs

LOV inhibits HMG-CoA reductase of the mevalonate-pathway resulting in the depletion of cholesterol and isoprenoids i.e., farnesyl-pp and geranylgeranyl-pp responsible for an inhibition of Ras and RhoA signaling, respectively. RhoA mediated inhibition of ROCK signaling induces p38MAPK activation, which in turn induces COX-2 mediated production of PPAR-γ activators i.e., 15d-PGJ2 via increased release of arachidonic acid (AA) from phospholipids (PP) metabolism by cPLA2. Subsequently, activated PPAR-γ induces PTEN which in turn inhibits PI3K-Akt signaling thus inhibits OPC proliferation via induction of the expression of cell cycle inhibitory proteins i.e., $p21^{Cip1}$ and $p27^{Kip1}$. These events subsequently induce the expression of myelin proteins leading to the differentiation of OPCs. Box depicts the mevalonate pathway, NT as neurotrophic factor, PKC as protein kinase C, SOX10 and sp1 as transcription factors. Pharmacological and biological agents used in the study are bolded (please see text for details).

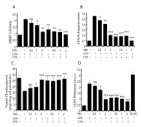

Fig. 2. LOV treatment is detrimental to OPCs under cholesterol/serum-deprived conditions

OPCs were cultured in Sato media for 24 h then treated with LOV (2 μM) for the next 48 h in the presence/absence of different FBS concentrations (%) including cholesterol (10 μM). Plots depict SREBP-2 activity (arbitrary units/mg of protein) (A), LDLR mRNA expression (arbitrary units) (B), level of cellular cholesterol (C) and cell death (D) in treated OPCs. Triton-X100 (0.05%) indicates 100% cell death (D). Results in plots are expressed as Mean ± SD of three independent experiments. Statistical significance is shown as *$p<0.05$, **$p<0.01$, ***$p<0.01$ and NS (non-significant) versus LOV alone.

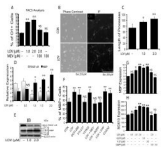

Fig. 3. Inhibition of RhoA-ROCK signaling promotes the phenotypic commitment and differentiation of OPCs

OPCs (2,000cells/cm^2) were cultured as described under 'Materials & Methods' and treated with LOV in the presence/absence of various pharmacological agents. Plot depicts percentage of $O1^+$ cell counts by FACS analysis at DIV4 (A). Representative fields of slides demonstrate $O1^+$ cells as revealed by phase-contrast (left panel) and fluorescence (right panel) microscopy (B). Plot depicts the length of processes (μm) in LOV treated OPCs (C). Plot depicts the level of PDGF-αR and MBP mRNAs (arbitrary units) in LOV-treated OPCs at DIV5 (D). Representative immunoblot depicts the level of PDGF-αR and MBP protein in LOV-treated OPCs at DIV7 (E). Plot depicts the percentage of MBP^+ cells analyzed by FACS analysis in OPCs treated with LOV (2 μM), mevalonate (MEV; 100 μM), farnesyl-pp (FPP; 5 μM), geranylgeranyl-pp (GGPP; 5 μM), and 3 μM each of the inhibitor of farnesyl transferase (FTI-277), geranylgeranyl transferase (GGTI-298), ROCK (Y27632) and RhoA (C3-exoenzyme, C3-EXZ) individually or in combinations at DIV7 (F). Plots depict the level of MBP (G) and SOX10 (H) mRNA (arbitrary units) in treated OPCs at DIV5. Results in plots are expressed as Mean ± SD of three independent experiments. Statistical significance is shown as *$p<0.05$, **$p<0.01$, and NS (non-significant) versus control (no-treatment).

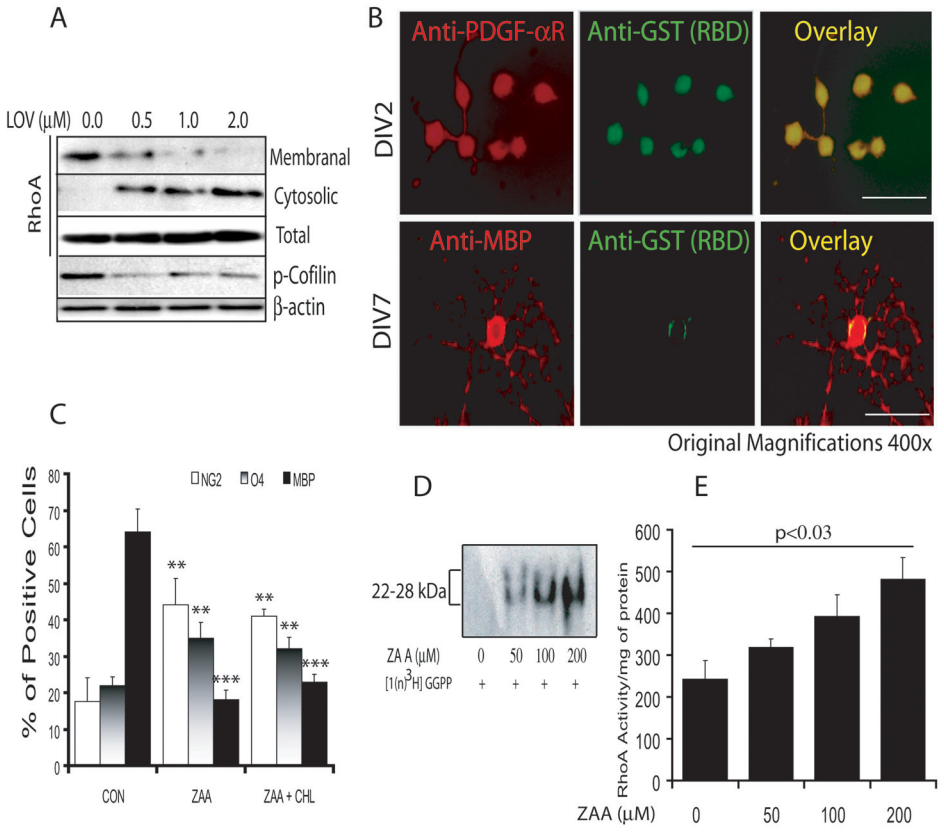

Fig. 4. Depletion of GGPP, but not FPP and cholesterol mediates the effect of LOV in OPCs

Cells were cultured and treated under conditions as described in Materials & Methods. Representative immunoblot of three independent experiments shows the level of RhoA (cytosolic and membranal fractions) and phosphorylated-cofilin in treated OPCs at DIV4 (A). Representative fields of slides depict activated RhoA in OPCs (at DIV2) and differentiated OLs (at DIV7) determined by double immunostaining using anti-GST along with anti–PDGF-αR or –MBP antibodies upon treatment with LOV (B). Plot depicts the percentage of NG2, O4 and MBP phenotype cells in OPC cultures treated with squalene synthase inhibitor zaragozic acid A (ZAA; 200 μM) as determined by FACS analysis at DIV7 (C). Representative autoradiograph of two independent experiments demonstrates the incorporation of [1(n)-^{3}H]-GGPP in ZAA-treated OPCs at DIV4 (D). Plot depicts RhoA activity (arbitrary units) in ZAA-treated OPCs in a dose-dependent fashion (E). Results in plots are expressed as Mean ± SD of three independent experiments. Statistical significance is shown as *p<0.05 and ***p<0.001 versus CON.

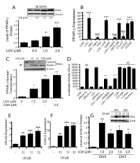

Fig. 5. LOV-mediated inhibition of RhoA-ROCK signaling induces transcriptional activation and expression of PPAR-γ

Cells were treated with LOV (2 μM) in the presence/absence of metabolites of the mevalonate-pathway or with inhibitors alone i.e., MEV (100 μM), 5 μM each of farnesyl-pp (FPP) and geranylgeranyl-pp (GGPP), and 3 μM each of the inhibitors of farnesyl transferase (FTI-277), geranylgeranyl transferase (GGTI-298), ROCK (Y27632) and RhoA (C3-exoenzyme, C3-EXZ) including PPAR-γ agonist, ciglitazone (CGN; 2 μM). Plot and representative immunoblot (insert) depict the level of PPAR-γ protein (arbitrary units) in OPCs at DIV4 (A). Plot depicts the expression of PPAR-γ mRNA (arbitrary units) in treated OPCs at DIV4 (B). Plot and representative blot (insert) depict PPAR-γ nuclear translocation (arbitrary units) in treated OPC at DIV2 (C). Plot depicts luciferase activity (RLU; relative light units/μg of protein) in B12 cells co-transfected with ptk-PPRE-*luc* and pRhoA-*dn* or pRhoA-*ca* plasmids or siRNA for PPAR-γ (siPPAR-γ) including transfected B12 cells with ptk-PPRE-*luc* and treated with 2 μM each of LOV, PPAR-γ antagonist (GW9662) and CGN, and 3 μM of each GGTI-298 and Y27632 for 24 h (D). Plots depict the expression of cPLA2 (E) and COX-2 (F) mRNA (arbitrary units) in treated OPCs with LOV at DIV4. Plot and representative immunoblot (insert) depict the level of COX-2 protein (arbitrary units) in treated OPCs (G). Results in plots are expressed as Mean ± SD of three independent experiments. Statistical significance *p<0.05, **p<0.01, ***p<0.001 versus control except D, where ***p<0.001 and NS (non-significant) were versus LOV.

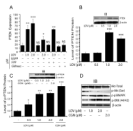

Fig. 6. LOV-mediated PPAR-γ activation induces PTEN expression in treated OPCs

Cells were treated with LOV in the presence/absence of geranylgeranyl-pp (GGPP; 5 μM), farnesyl-pp (FPP; 5 μM) and PPAR-γ antagonist (GW9662; 2 μM) or ciglitazone (CGN) alone. Plot depicts the level of PTEN mRNA (arbitrary units) in treated OPCs at DIV4 (A). Plot and representative immunoblot (insert) depict the level of PTEN protein (arbitrary units) in treated OPCs at DIV4 (B). Plot and representative immunoblots (insert) depict the level of phosphorylated PTEN (arbitrary units) in treated OPCs at DIV4 (C). Representative immunoblot depicts the level of Akt/p-Akt (Ser), p-p38MAPK and p-ERKs (44/42) in treated OPCs at DIV4 (D). Results in plots are expressed as Mean ± SD of three independent experiments. Statistical significance *p<0.05, **p<0.01, ***p<0.001 and NS (non-significant) versus untreated cells.

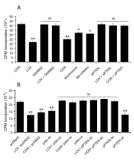

Fig. 7. Activation of PPAR-γ and PTEN cascade inhibits the proliferation of LOV treated B12 cells

Cells were treated with LOV and different agents or transfected with different plasmids or siRNAs. Plot depicts the effect of LOV (2 μM), GW9662 (3 μM), ciglitazone (CGN; 2 μM), PI3K inhibitor (wortmannin; 5 nM) and Akt inhibitor (5 μM) on the proliferation of B12 cells (24 h) using [H^3] thymidine incorporation analysis including those B12 cells transfected with siRNA for PTEN (siPTEN) and treated with LOV and CGN (A). Plot depicts the proliferation of transiently transfected B12 cells with pcDNA3, pPTEN-*dn*/*wt* or pAkt-*dn*/*ca* plasmids (24 h) using [H^3] thymidine incorporation analysis after treatment with LOV (2 μM) or CGN (2 μM) (B). Results in plots are expressed as Mean ± SD of 3 independent experiments. Statistical significance *$p < 0.05$, **$p<0.01$ and NS (non-significant) versus CON (A) or pcDNA3 (B).

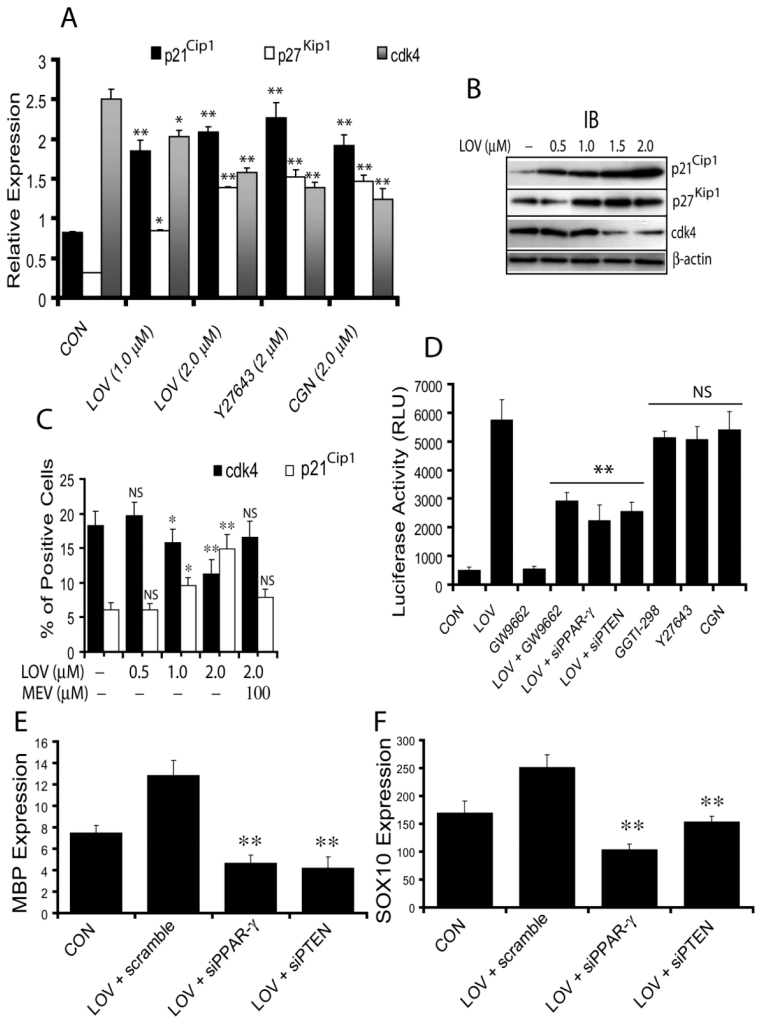

Fig. 8. Activation of PPAR-γ and PTEN induces cell cycle arrest at G1

Cells were cultured and treated with different pharmacological agents. Plot depicts the expression of $p21^{Cip1}$, $p27^{Kip1}$ and cdk4 mRNA (arbitrary units) in treated OPCs at DIV4 (A). Representative immunoblots depict the level of cell cycle inhibitory proteins in treated OPCs at DIV4 (B). Plot depicts the percentage of $cdk4^{+}$ and $p21^{Cip1+}$ cells in treated OPCs at DIV4 determined by FACS analysis (C). Plot depicts luciferase activity (RLU; relative light units/μg of protein) in transiently transfected B12 cells with MBP-P6L3-*luc* plasmids and treated with 2 μM each of LOV, antagonist (GW9662) and agonist (CGN) of PPAR-γ and, inhibitors of geranylgeranyl transferase (GGTI-298) and ROCK (Y27632) including co-transfection with siRNA for PPAR-γ (siPPAR-γ) or PTEN (siPTEN) and treatment with LOV (D). Plots depict the level of MBP (E) and SOX10 (F) mRNAs (arbitrary units) in transiently transfected OPCs (as indicated) and treated with LOV. Results in plots are expressed as Mean ± SD of three independent experiments. Statistical significance *$p<0.05$, **$p<0.01$ and NS versus CON (for A and C) or LOV (for D) or LOV + scramble (for E and F).

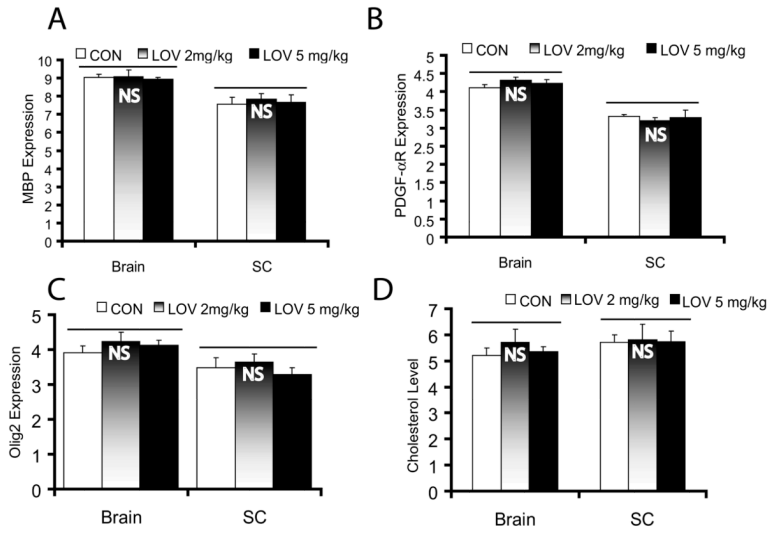

Fig. 9. Expression of OPC/OL proteins and the level of cholesterol in the CNS of chronically treated normal rats with LOV

Normal Lewis female rats (n = 6 each group) were treated with LOV (2 mg/kg and 5 mg/kg, ip) every day for 6 months as described in §Materials & Methods. Plots depict the level of MBP (A), PDGF-αR (B) and olig2 (C) mRNAs (arbitrary units) including the level of cholesterol (μg/mg of protein) (D) in the brain and spinal cord (SC) tissues of LOV-treated/ untreated rats. Results in plots are expressed as Mean ± SD. Statistical significance non-significant (NS) versus CON.

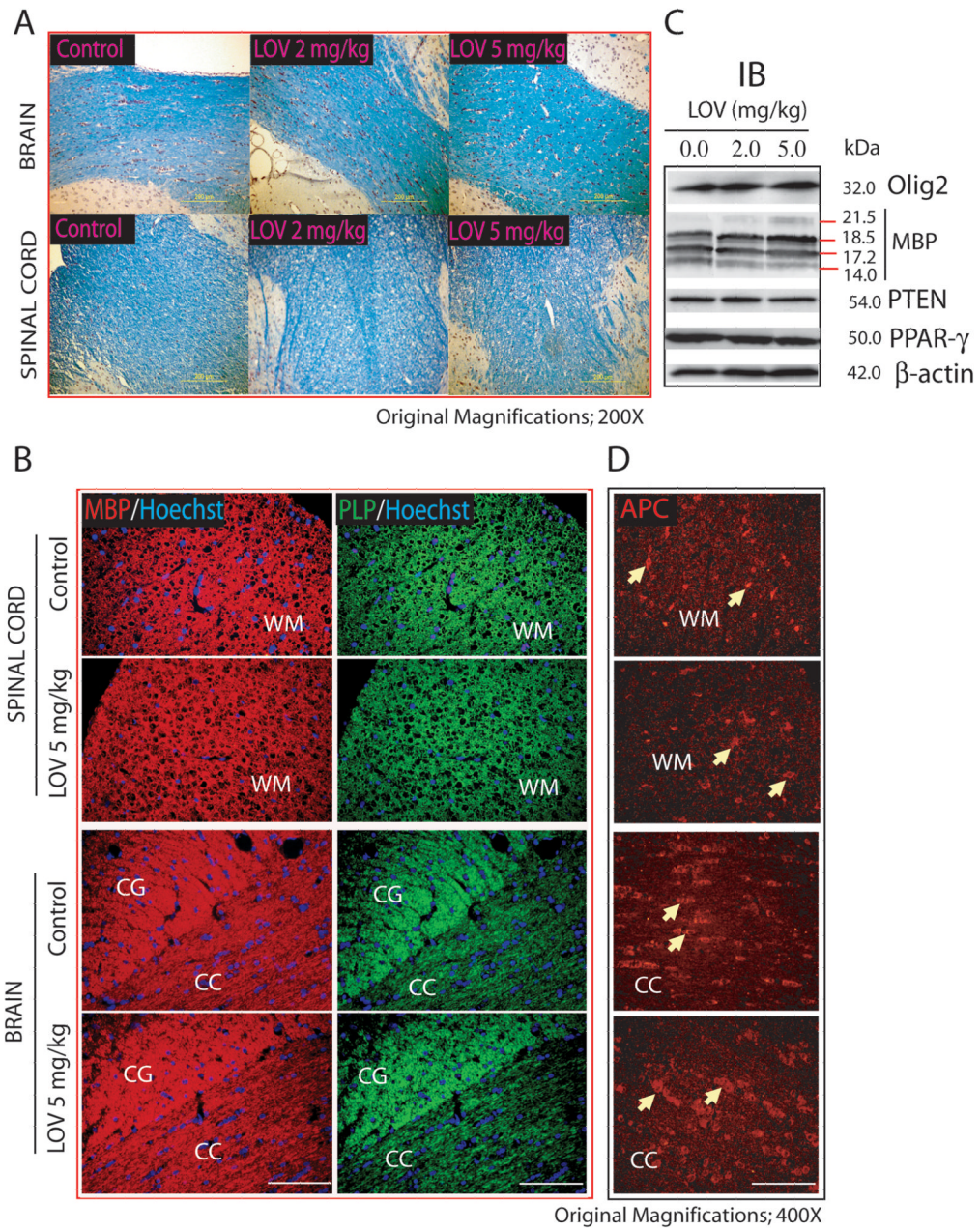

Fig. 10. Myelin integrity and count of OLs in the CNS of chronically treated normal rats with LOV

Representative field of luxol fast blue (LFB) stained sections demonstrates myelin integrity in the white matter regions i.e., corpus-callosum (CC) of the brain and dorsal funiculum (DF) of the spinal cord of rats (A). Representative field of the sections depicts immunostaining for MBP and PLP in the dorsolateral funiculum of the spinal cord (upper panel) and cingulum (CG) and corpus-callosum (CC) regions of the brain (lower panel) (B). Representative immunoblot depicts the level of proteins in the SC tissue of LOV treated/ untreated rats (C). Representative field of the sections depicts APC^+ OLs in the white matter (WM) of dorsolateral funiculum of the spinal cord (upper pane) and CC of the brain (lower panel) (D). Arrowhead depicts the APC^+ mature OLs in the WM and CC of spinal cord and

brain, respectively. Hoechst dye was used as counter stain to visualize nuclei in the sections (B).

Table 1

List of primers used for quantitative real-time PCR analysis

Gene Name	Primer Sequence
GAPDH	FP: 5’-ggaggaatgggagttgctgttgaa-3’; RP: 5’-ggaggaatgggagttgctgttgaa-3’
18S rRNA	FP: 5’-ccagagcgaaagcatttgccaaga-3’; RP: 5’-tcggcatcgtttatggtcggaact-3
LDLR	FP: 5’-ttgtcctgtttcacaacgtcacgc-3’; RP: 5’-atgtccttggccagtagcatacca-3’
PDGF-αR	FP: 5’-cagacattgaccctgttccagagg-3’; RP: 5’-gaatctatgccaatatcatccatc-3’
MBP	FP: 5’-ctctggcaaggactcacacac-3’; RP: 5’-tctgctgagggacaggcctctc-3’
Olig2	FP: 5’-tcaagtcatcttcctccagcacct-3’; RP: 5’-ggctcagtcatctgcttcttgtct-3’
SOX10	FP: 5’-tctacacggccatctctgacc-3’; RP: 5’-tcgtatatactggctgttcccagtg-3’
PTEN	FP: 5’-agagcgtgcggataatgacaagga-3’; RP: 5’-tggagagaagtatcggttggcctt-3’
PPAR-γ	FP: 5’-agatcatctacaccatgctggcct-3’; RP: 5’-aggaactccctggtcatgaatcct-3’
COX-2	FP: 5’-atcgatgccatggaactgtatccc-3’; RP: 5’-ctcttacagctcagttgaacgcct-3’
cPLA2	FP: 5’-cctgatgtggagaaggattgcaca-3’; RP: 5’-ttccttggtttccctcagaacacc-3’
$p21^{Cip1}$	FP: 5’-tggtcttctgcaagagaaagccct-3’; RP: 5’-atgaaggctaaggcagaagatggg
$p27^{Kip1}$	FP: 5’-agcttgcccgagttctactacaga-3’; RP: 5’-tttgcctgagacccaattgaaggc-3’
cdk4	FP: 5’-gttgctggaaatgctgacctt-3’; RP: 5’-gtcactttcctccttgtgcaggta-3’

Note; FP stands for forward primer and RP stands for reverse primer.